Random and exchange anisotropy in consolidated nanostructured Fe and Ni: Role of grain size and trace oxides on the magnetic properties

Jörg F. Löffler
Paul Scherrer Institut, CH-5232 Villigen PSI, Switzerland

Jürg P. Meier, Bernard Doudin, and Jean-Philippe Ansermet
Institut de Physique Expérimentale, EPFL Lausanne, CH-1015 Lausanne, Switzerland

Werner Wagner
Paul Scherrer Institut, CH-5232 Villigen PSI, Switzerland

(Received 2 July 1997)

Results of magnetization measurements on nanocrystalline Fe and Ni produced by inert-gas condensation are presented. The grain size, which is about 10 to 20 nm in the as-prepared state, is increased by annealing the samples incrementally from 100 °C to 1000 °C. The coercive field shows a pronounced variation with grain size, with a maximum at around 30 nm and a steep decrease for smaller grain sizes. The coercivity is discussed on the basis of the random-anisotropy model that predicts that the effective anisotropy constant is reduced by averaging over magnetically coupled grains. This behavior is observed as long as the grain size is smaller than the effective bulk domain-wall width. The model also accounts for the approach to saturation in nanostructured Fe yielding values for the ferromagnetic correlation length and the anisotropy constant of the grains. The latter is about four times higher than the bulk value of Fe. Hysteresis measurements at 5 K after field cooling show a shift and broadening of the hysteresis loops for both Fe and Ni, which is attributed to an exchange coupling between the ferromagnetic grains and antiferromagnetic or ferrimagnetic (oxide) interfacial phases. The hysteresis shift decreases and finally vanishes with increasing grain size. This is indicative of a restructuring of the oxides, which is confirmed by the coercive field of the Fe samples showing a step at about 120 K caused by a phase transition of Fe_3O_4. The step vanishes again with further increasing grain size. The saturation magnetization of the Ni samples increases with increasing annealing temperature, a fact that is attributed to the evolution of the oxides also. [S0163-1829(98)00505-0]

I. INTRODUCTION

In conventional ferromagnetic polycrystalline materials with grain sizes in the μm regime the width of a domain wall is typically several tens of nanometers. In nanostructured materials, i.e., in materials with grain sizes in the nanometer range, when the grain size becomes comparable to or is even smaller than the width of a domain wall, the magnetic properties are expected to undergo fundamental changes.

Individual ferromagnetic small particles are generally divided into three size categories.[1–3] To the first category belong particles that are sufficiently large to contain several domains and where the magnetization reversal is determined by domain-wall motion, a mechanism that is relatively unimpeded by imperfections and leads to low coercive fields. With decreasing particle size, the particle finally contains only one domain. This second category contains particles for which a rigid rotation of the magnetization vector is the only possible reversal process. The rotation of the magnetization of the entire particle is in general associated with a large change in energy (depending on the anisotropy energy of the particle) such that single-domain particles usually have large coercive fields. As the particle size decreases further, they enter into the third category (Ref. 4) where the thermal energy at the temperature of the experiment is sufficient to equilibrate the magnetization of the entire particle in a time short compared with that of the experiment. In this case the ensemble of particles acts as a paramagnet with relatively large but unordered individual moments. Such a behavior is known as superparamagnetism in the literature.[1,5–7]

The above characterization refers to isolated particles. The situation is different when the particles are in contact, which is the case in consolidated nanostructured materials.[8] A magnetic exchange interaction across the interfaces is then possible. When the grain size of such materials is comparable to the effective bulk domain-wall width, the magnetization may not follow the randomly oriented easy axis of each individual grain, and a common alignment of the magnetization in correlated grains may occur. The magnetocrystalline anisotropy constant may then be averaged over several grains with the consequence that the coercive field decreases with decreasing grain size. This model is known as the random-anisotropy model (RAM).[9–11] It was originally developed for amorphous ferromagnetic materials. Recently, it was also applied to nanostructured Fe films obtained by cluster beam deposition.[12]

In addition to these microstructure-related effects, the magnetic properties may be affected by local structural features in the grain boundaries. The average magnetic moment of grain-boundary atoms can be different from the one of atoms on regular crystal lattice sites. Indeed, a reduction of the saturation magnetization compared with the bulk value has been conjectured for nanocrystalline Ni,[13] although later investigations on nanocrystalline Ni with lower oxygen

content[14] did not show a change of the saturation magnetization with decreasing grain size.

When transition metals like Fe, Ni, and Co are produced by inert-gas condensation[15,16] the clusters prior to consolidation are exposed to the residual gas atmosphere of the recipient where they can readily absorb oxygen. When the samples are taken out of the recipient after consolidation, it is still likely that oxygen (and other non-noble gases) can reach inner surfaces by migration through open channels or diffusion in grain boundaries. Hence, the influence of oxidation has to be taken into consideration.

We performed magnetization measurements on nanostructured Fe and Ni produced by inert-gas condensation in order to characterize the magnetic properties of consolidated nanosized grains. We measured the coercive field, the remanent and the saturation magnetization systematically for grain sizes between 10 and 100 nm at temperatures between 5 and 300 K. We compared our experimental results with the theoretical predictions of the RAM.[9–11] We show that the RAM can successfully be applied to nanostructured materials. We also characterized the presence of oxides by detecting an exchange interaction between the ferromagnetic phase and antiferromagnetic or ferrimagnetic oxide interfacial phases.

II. EXPERIMENTAL PROCEDURE

A. Sample preparation

The Ni and Fe samples were produced by the inert-gas condensation technique.[15,16] The material was thermally evaporated from a tungsten boat in a 10^{-6} Pa base pressure vacuum system filled with 100 Pa of 99.999% pure He gas. During the inert-gas condensation process the atoms in the vapor phase condense to form small nanometer-sized crystallites that are collected on a rotating cylinder cooled by liquid nitrogen. The powder is scraped off into a funnel and transferred to a compaction device connected to the same vacuum recipient. After reevacuation to the initial pressure of 10^{-6} Pa the powder is consolidated by pressing at a pressure of 1 to 1.2 GPa. Typical consolidation parameters are given in Table I. The samples are disk-shaped with a diameter of 8 mm and a thickness of 100–300 μm.

B. Sample characterization

The *density* of the samples was determined by the Archimedes immersion method. The relative geometrical densities $\rho_{\mathrm{geo}}/\rho_{\mathrm{lit}}$, which include the density reduction resulting from open porosity, are listed in Table I for the respective samples in the as-prepared state.

Metallic impurities, measured by energy-dispersive x-ray analysis (EDX) in a scanning electron microscope, were found in total lower than 0.5 at. % for all samples. Not surprisingly, the boat material tungsten was detected as the dominating impurity.

The *oxygen content* of the as-prepared samples, also detected by EDX (the EDX system was equipped with an ultrathin window allowing the detection of light elements down to boron), was at most 6 at. % in Ni and 12 at. % in Fe. Hot extraction performed on two Ni samples provided 6 ± 1 at. % of light elements (H, N, and O). Obviously, a certain oxygen content is inherently introduced either during the synthesis procedure, although the basic vacuum of the recipient is in the 10^{-6} Pa range, or by oxygen resorption in the consolidated state after exposure to air.

TABLE I. Consolidation conditions and characteristic structural parameters of representative samples of nanostructured Fe and Ni used in the present study; the table shows further the average grain size D and lattice strain e as well as the relative geometrical density $\rho_{\mathrm{geo}}/\rho_{\mathrm{lit}}$.

	Consolidation parameters	D [nm]	e [%]	$\rho_{\mathrm{geo}}/\rho_{\mathrm{lit}}$
Fe, sample #1 as-prepared	1.2 GPa, RT, 2 h	10	0.52	0.80
Fe, sample #2 as-prepared	1.2 GPa, RT, 2 h	9	0.63	0.80
Fe, sample #3 as-prepared	1 GPa, 200 °C, 2 h	24	0.37	0.84
Fe, sample #4 as-prepared	1 GPa, 200 °C, 2 h	24	0.35	0.83
Fe, sample #5 as-prepared	0.6 GPa, RT, 0.25 h	21	0.16	0.68
Ni, sample #1 as-prepared	1.2 GPa, RT, 2 h	14	0.40	0.85
Ni, sample #2 as-prepared	1.2 GPa, RT, 2 h	15	0.42	0.85
Ni, sample #3 as-prepared	1 GPa, 200 °C, 2 h	20	0.29	0.87
Ni, sample #4 as-prepared	1 GPa, 200 °C, 2 h	20	0.28	0.86

To determine the grain size of the samples, x-ray diffraction (XRD) patterns were recorded with Cu K_α radiation; for examples see Fig. 1. The *average grain size D* and the *lattice strain e* were determined from the most intensive peaks of first and second order, i.e., (110) and (220) for Fe and (111) and (222) for Ni, evaluating the integral breadths of the Bragg peaks by the method described in Ref. 17, assuming Gaussian strain and Cauchy size broadening [e is a ''maximum strain'' and is related to the more commonly used root-mean-square lattice strain $\langle \epsilon^2 \rangle^{1/2}$ by $e = 1.25 \langle \epsilon^2 \rangle^{1/2}$ (Ref. 17)]. The values for the as-prepared samples are included in Table I.

C. Sample processing

In order to induce grain growth, the samples were annealed in successive steps up to a final temperature of 700 °C (1000 °C) in a tube furnace at a pressure of 10^{-4} Pa, for 24 h at each temperature. As an example, the grain size and lattice strain as a function of annealing are plotted in Fig. 2 for the nanostructured sample Fe #2. Up to 200 °C the grain size increases only slightly but the lattice strain is significantly relieved. At higher temperatures a more rapid grain growth is induced. In conjunction with the grain growth the relative geometrical density of this sample also increased from initially 80% to 87.5% for the different annealing steps between 100 °C and 600 °C. The x-ray pattern did not resolve oxygen peaks in any of the as-prepared samples except

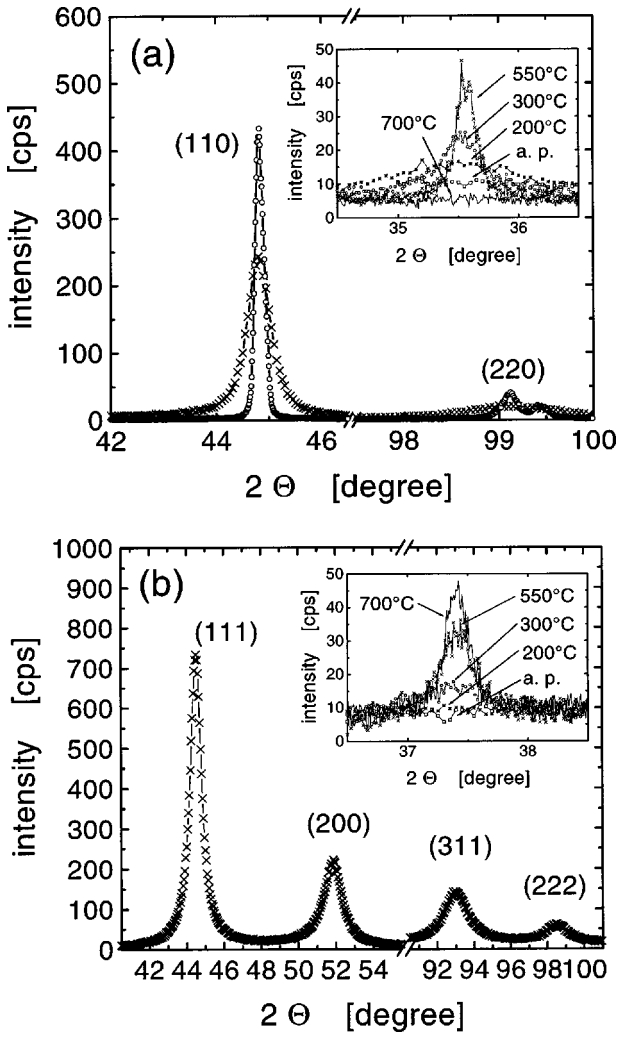

FIG. 1. X-ray diffraction pattern of (a) nanocrystalline sample Fe #3, as-prepared (crosses) and after annealing at 700 °C (circles, intensity scale reduced by a factor of 4), inset: (311)-peak of cubic Fe_3O_4 (magnetite) as a function of annealing (annealing temperatures given in the figure; a.p.=as-prepared); (b) nanocrystalline Ni #3, as-prepared, inset: (111)-peak of cubic NiO (bunsenite) as a function of annealing.

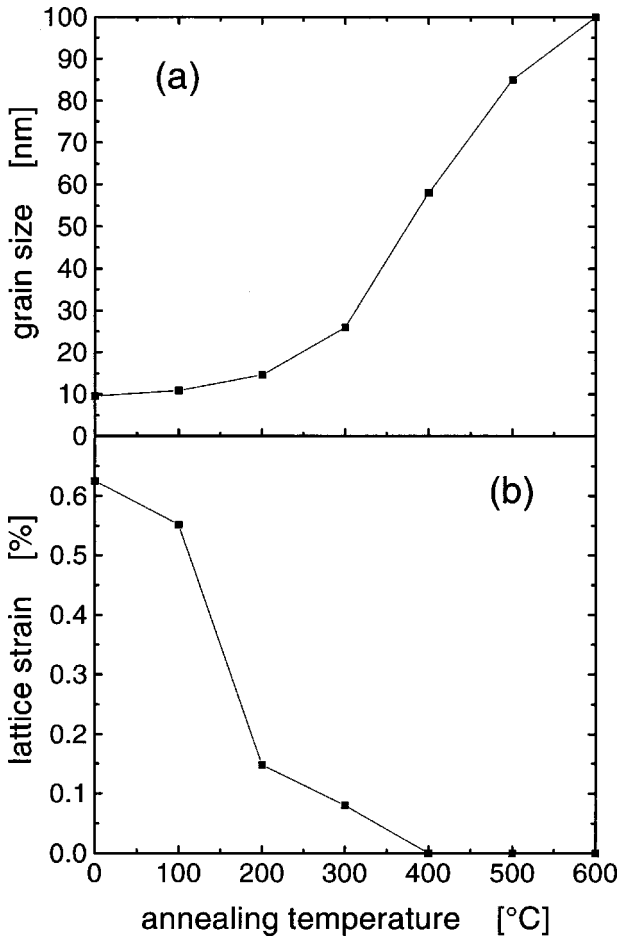

FIG. 2. Change of the average grain size D (a) and of the lattice strain e (b) as a function of annealing for a selected sample (sample #2) of nanostructured Fe.

in one sample that was consolidated at a lower pressure of only 0.6 GPa (Fe #5, Table I). Here, oxide peaks of Fe_3O_4 (magnetite) were found.

After annealing, XRD of the Fe samples (except Fe #5) shows a broad Fe_3O_4 ''oxide hump'' developing for low annealing temperatures [inset in Fig. 1(a)], which narrows to an Fe_3O_4 peak for annealing temperatures above 300 °C. After annealing at 700 °C the Fe_3O_4 peak vanishes owing to the formation of FeO that is stable above 560 °C.[18] Likewise, XRD of Ni also develops a broad NiO ''oxide hump'' that narrows to a peak for annealing temperatures above 550 °C [inset in Fig. 1(b)].

D. Magnetization measurements

The magnetization measurements were performed with a commercial superconducting quantum interference device magnetometer on samples in the as-prepared state and after each annealing step. The coercive field, the remanent and the saturation magnetization of all samples were measured at temperatures between 5 and 300 K at the different steps of annealing. The data presented correspond to sequences of measurements and accumulative annealing steps performed on a given sample.

III. EXPERIMENTAL RESULTS AND DISCUSSION

The general shape of the hysteresis loops did not change as a function of annealing or measurement temperature. In particular, the low remanent magnetization determined by demagnetizing effects followed the evolution of H_c on which we concentrate in the following.

We will first present the results obtained from Fe. The coercive field H_c was measured as a function of temperature, following different steps of the annealing process that induced grain growth (for reasons of clarity, the annealing temperature is given in °C and the measurement temperature in K). Consider for example sample Fe #1 in Fig. 3(a). Starting from the as-prepared state, the coercive field first increases with increasing annealing temperature, reaches a maximum after annealing at 200 °C and then decreases after further annealing down to a few Oe. This trend is followed at all temperatures at which the specimen was measured. After annealing at 100 °C we observe that the coercive field shows a broad maximum around a measurement temperature of 25 K

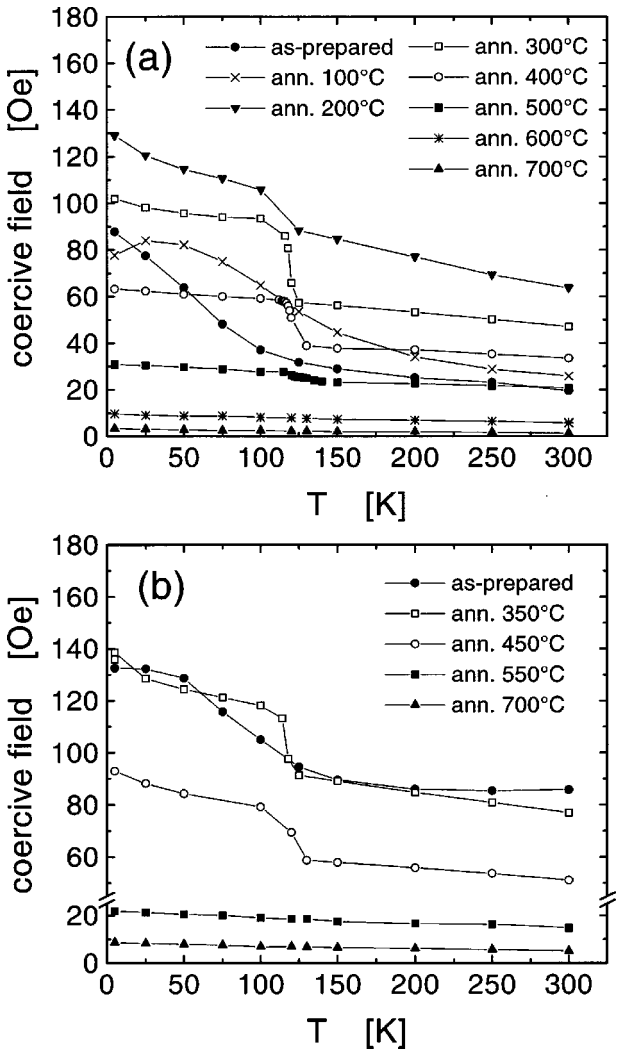

FIG. 3. Coercive field measured on two samples of nanostructured Fe [(a) sample #1 and (b) sample #4] as a function of measurement temperature in the as-prepared state and following different annealing steps.

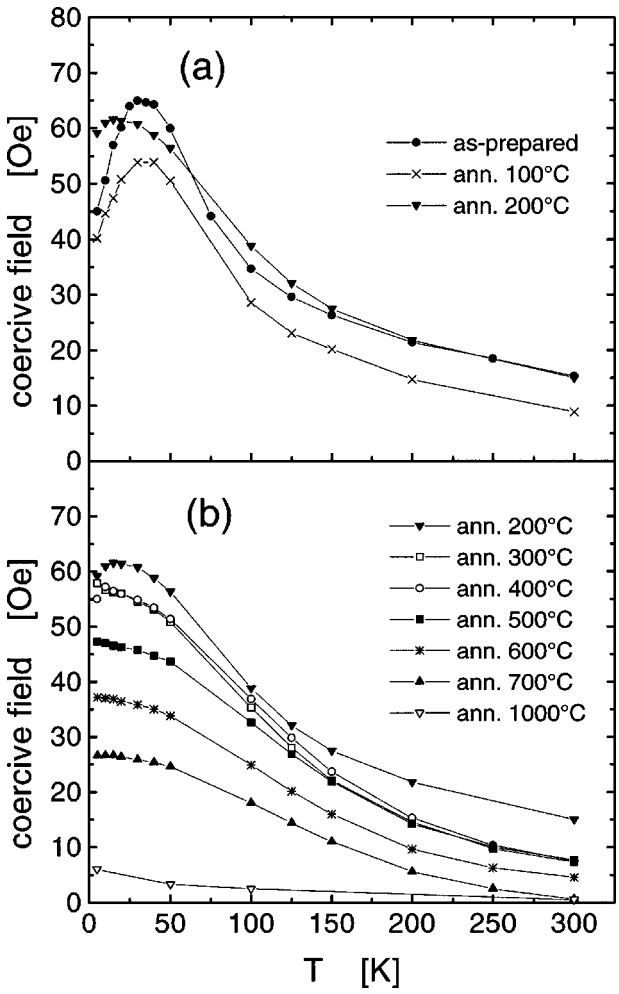

FIG. 4. Coercive field of nanostructured Ni (sample #2) as a function of temperature in the as-prepared state and for different annealing steps [presented in Figs. (a) and (b) for the benefit of clarity].

whereas for all other annealing steps the coercive field decreases or remains constant in this range. A second, remarkable observation is a pronounced step in H_c at about 120 K, which develops with increasing annealing temperature and is largest for the sample annealed at 300 °C. Further annealing leads to a broadening, lowering, and finally to the disappearance of the step.

This general trend in the temperature dependence of H_c occurred reproducibly in all Fe samples investigated. Figure 3(b) shows the example of sample Fe #4 that had undergone a consolidation by pressing at 200 °C (Table I). This compaction yields a coercivity that remains essentially unchanged in magnitude by the annealing at 350 °C but develops the same step at 120 K. With further annealing above 350 °C, the step vanishes and the coercive field decreases in magnitude, tending towards the values of polycrystalline Fe.

The coercive field H_c of nanocrystalline Ni shows trends similar to that of the Fe samples as shown for example by the sample Ni #2 (Fig. 4). A maximum in H_c at about 25 K is observed in the as-prepared state and after annealing at 100 °C (Fig. 4). For higher annealing temperatures, this maximum is less pronounced and finally vanishes. As opposed to the case of nanocrystalline Fe, H_c decreases after the first annealing step at 100 °C, compared to the as-prepared state. Upon further annealing, however, the coercive field increases again, similar to Fe, and passes a flat maximum with annealing at about 200 °C. The experimental results have been reproduced for the other Ni samples of Table I.

A. Effect of grain size: Random anisotropy

Each annealing treatment resulted in a grain growth as shown in Fig. 2(a) for the sample Fe #2. We can attribute a grain size to the corresponding annealing temperature for each sample. Thus, the evolution of the coercive field can be expressed as a function of grain size. Figure 5 shows the collected data of all our Fe samples. We find a continuous increase of the coercive field with decreasing grain size from 100 nm down to a size of about 30 nm, and then a sharp decrease as the grain size decreases further.

An increase in coercivity with decreasing grain size, approximately following a $H_c \sim 1/D$ behavior, was observed in polycrystalline materials and was explained by domain-wall pinning at grain boundaries[19] that becomes progressively

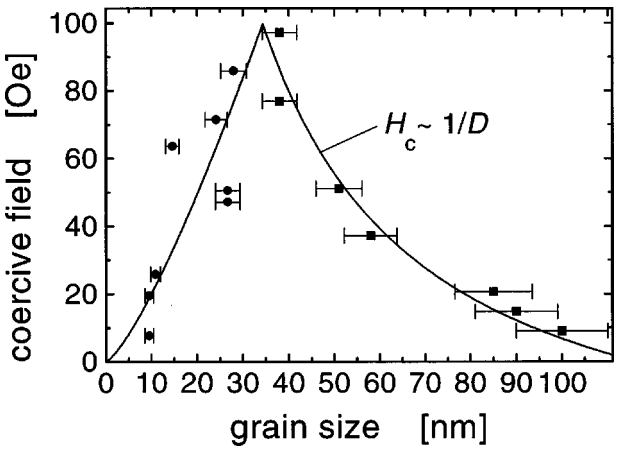

FIG. 5. Coercive field for different samples of nanostructured Fe as a function of grain size, measured at a temperature of 300 K. The solid curve is primarily a guide to the eye visualizing the general trend of the data, but also represents a $1/D$ behavior for grain sizes larger than 30 nm.

more efficient as the volume fraction of grain boundaries increases. A $1/D$ behavior of the coercive field was measured on coarse-grained polycrystalline Fe (Ref. 20) and Ni-Fe and Co-Fe alloys.[21] Recalling that the effective width of a domain wall in coarse-grained Fe is 46 nm [calculated from $\delta_w = \pi\sqrt{A/K_{\text{bulk,Fe}}}$ with $K_{\text{bulk,Fe}} = 4.7\times 10^5$ erg/cm^3 (Ref. 22) and the exchange constant $A = 10^{-6}$ erg/cm (Ref. 23)], we expect single-domain grains as the stable configuration in the size range around 46 nm, and presumably also up to a size scale several times larger than δ_w. In this regime in our nanostructured materials we still find a $1/D$ behavior down to a grain size of 30 nm (Fig. 5). Thus, the observed $1/D$ dependence suggests that the change in magnetization direction still occurs via a process similar to domain-wall motion at sizes down to 30 nm.

Below 30 nm, we find a steep decrease of H_c towards smaller grain sizes (Fig. 5). This decrease can be explained by the random-anisotropy model.[9–11,24] In consolidated materials, exchange coupling between neighboring grains is possible and may overcome the magnetocrystalline anisotropy of each grain. This exchange coupling results in a reduced effective anisotropy $\langle K\rangle$, which represents an average over the magnetocrystalline anisotropies of the correlated grains. For a random orientation of the anisotropy axes of the grains the effective anisotropy is reduced by a factor of $1/\sqrt{N}$, where N is the number of the magnetically correlated grains. Consequently, one expects a decrease of the anisotropy energy and therefore also a decrease of the coercive field with decreasing grain size.

In the following, we apply the theoretical predictions of the RAM to our magnetization measurements on nanostructured Fe and Ni. The key parameters of the RAM are the local anisotropy field

$$H_r = \frac{2K_r}{M_s} \tag{1}$$

and the effective exchange field

$$H_{\text{ex}} = \frac{2A}{M_s R_a^2}, \tag{2}$$

where K_r is the anisotropy constant of the single grains, M_s is the saturation magnetization and A is the exchange constant. R_a is the distance over which the anisotropy axes are correlated. The ferromagnetic correlation length R_f tends to extend over much larger distances than R_a. The value of R_f is obtained by minimizing the sum of the exchange and anisotropy energy, $E_{\text{ex}} + E_r$, with respect to R_f. With $E_{\text{ex}} \sim AV/R_f^2$ and $E_r \sim -K_r V/\sqrt{N}$, where $N = (R_f/R_a)^3$, one obtains $R_f \sim A^2/(R_a^3 K_r^2) \sim R_a H_{\text{ex}}^2/H_r^2$. The minimum energy itself is proportional to $M_s V H_r^4/H_{\text{ex}}^3$, i.e., proportional to R_a^6. Equating this minimum energy to $M_s H_c V$ (as stated for example in Ref. 9) leads to an estimate for the coercive field of the form

$$H_c \sim \frac{K_r^4}{A^3 M_s} R_a^6. \tag{3}$$

In nanocrystalline materials, R_a is equal to the grain size. The dependence of H_c on grain size in agreement with Eq. (3) was illustrated in Refs. 25 and 26. The data were obtained from nanocrystalline soft magnetic Fe-based alloys combining results from different materials with coercive fields that are orders of magnitude apart from each other. From our data based on Fe alone, the range in grain size and coercive field that we were able to cover was too small to verify explicitly a dependence of the coercive field proportional to R_a^6 $(=D^6)$. However, we obtain a sharp increase of the coercive field up to a grain size of about 30 nm, in general agreement with Eq. (3).

For a further check of the applicability of the RAM to our nanostructured materials we investigated the magnetization of nanostructured Fe in approach to saturation. In the formalism of the RAM the magnetization as a function of the external field H is expected to show a characteristic behavior of the form[10]

$$\frac{M}{M_s} = 1 - \frac{\lambda^2}{30p}\int_0^\infty dx\; e^{-px} x^2 C(x)$$

$$\text{with}\;\; p^2 = \frac{H}{H_{\text{ex}}} \;\;\text{and}\;\; \lambda = \frac{H_r}{H_{\text{ex}}} = \frac{K_r R_a^2}{A}. \tag{4}$$

$C(x)$ is a correlation function describing the distance over which the anisotropy axes are correlated, scaled with $C(0) = 1$ and $C(x = r/R_a \gg 1) = 0$. By assuming that $C(x)$ is a step function, i.e., $C(x \leqslant 1) = 1$ and $C(x > 1) = 0$, we obtain from Eq. (4),

$$M = M_s\left\{1 - \frac{\lambda^2}{30p^4}\left[2 - e^{-p}(2 + 2p + p^2)\right]\right\}. \tag{5}$$

A different expression, assuming an exponentially decaying correlation function $C(x) = \exp(-x)$, can be found in Refs. 12 and 27.

In order to check the applicability of Eqs. (4) and (5), we carefully measured the approach to saturation for the as-prepared sample Fe #1 at 5 K. The curves measured for different orientations of the sample with respect to the ap-

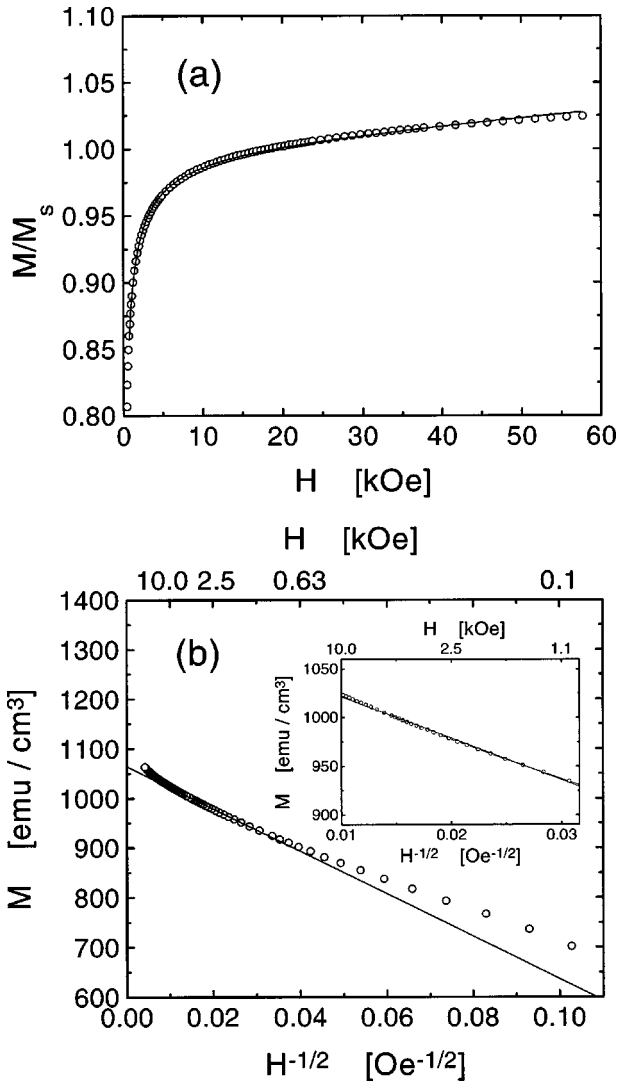

FIG. 6. Magnetization curve for nanostructured Fe (sample #1); (a) linear presentation in which the solid curve represents a fit according to the RAM [Eq. (5)] including the magnetization terms contributing at high fields ($H \gg H_{ex}$) and (b) plotted vs $H^{-1/2}$, where the straight line represents the $H^{-1/2}$ dependence of the magnetization. This line [Eq. (6)] was fitted to the data at intermediate fields (cf. inset).

plied field were corrected using the geometrical demagnetizing factors and $M_s = 1040$ emu/cm^3. This correction led to a satisfactory superposition of the curves measured for the different orientations in the range of interest, i.e., $M/M_s > 0.8$. The so corrected data were fitted using Eq. (5), extended by an additional term proportional to H in order to account for the observed susceptibility at high fields (see also Ref. 27). Figure 6(a) shows the results of the fit to the experimental data, from which we deduce $\lambda = 2$ and $H_{ex} \approx 10^4$ Oe. No reasonable fit was possible using the exponential correlation function $C(x) = \exp(-x)$. From the value of λ, we obtain $K_r = 2 \times 10^6$ erg/cm^3 using the bulk value $A = 10^{-6}$ erg/cm (Ref. 23) for the exchange constant and $D = 10$ nm for R_a.

In the two limiting regimes $H \ll H_{ex}$ ($p \ll 1$) and $H \gg H_{ex}$, Eq. (4) is not sensitive to the form of $C(x)$ and one obtains for the change in magnetization $\delta M = M_s - M$ for $H \ll H_{ex}$ (Ref. 28)

$$\frac{\delta M}{M_s} = \frac{\Omega}{120\pi}\frac{\lambda^2}{p} \sim \frac{1}{\sqrt{H}} \text{ with } \Omega = R_a^3 \int d^3x C(x). \quad (6)$$

Ω is the volume inside which the anisotropy axes are correlated. Figure 6(b) shows the magnetization M versus $H^{-1/2}$ to illustrate the field range where Eq. (6) describes the $H^{-1/2}$ dependence for intermediate fields in the regime $H \ll H_{ex}$. From the slope of the straight line in this plot, applying Eq. (6), we again obtain a value of $\lambda = 2$, consistent with the result of the entire fit with a step function [Eq. (5)].

The anisotropy constant $K_r = 2 \times 10^6$ erg/cm^3 is four times higher than the value for coarse-grained polycrystalline Fe [$K_{bulk,Fe} = 4.7 \times 10^5$ erg/cm^3 (Ref. 22)] in agreement with the higher values obtained from investigations on small isolated Fe particles.[7,12,29] The characteristic $H^{-1/2}$ behavior has also been observed in amorphous Fe-Sm-B alloys[30] and in amorphous Fe.[31]

With our fitted results we can calculate the ferromagnetic correlation length R_f, using the expression[10]

$$R_f = \frac{36\pi}{\Omega}\left(\frac{A}{K_r}\right)^2. \quad (7)$$

Assuming for $C(x)$ again a step function, we obtain $R_f = 27 R_a/\lambda^2 = 70$ nm ($\gg D = 10$ nm), consistent with the ferromagnetic correlation length obtained from small-angle neutron scattering performed on the same samples.[32]

Using the arguments of Ref. 33 it can be shown that with free boundary conditions no 180° domain-wall-type solutions can exist on length scales shorter than[34] $L_0 = \pi\sqrt{A/K}$ ($= \pi R_a/\sqrt{\lambda}$). Using the bulk values for A and K the critical length scale L_0 is equal to the effective domain-wall width $\delta_w = 46$ nm. From the fits in approach to saturation [Eqs. (5) and (6)] we obtain ($\lambda = 2$) $L_0 = 22$ nm. This grain-size regime represents the upper limit of the RAM and agrees well with the grain size of about 30 nm for which we observe the maximum of H_c (Fig. 5).

In the case of Ni, the first annealing step at 100 °C induces a reduction of the coercive field (Fig. 4) as opposed to the case of nanocrystalline Fe. After this annealing step the grain size increased only slightly (from 15 to 17 nm) but the value of the strain reduced by one half (from 0.42% to 0.22%). In terms of the RAM, a decrease in H_c indicates an enhanced magnetic coupling with the consequence that the effective anisotropy constant $\langle K \rangle$ is reduced further by averaging over a larger number of coupled grains. The healing of imperfections at grain boundaries and interfaces after the first annealing step (as also suggested in Ref. 14) is very likely to be the reason for the reduction of H_c. Upon further annealing, the coercive field increases, passes a flat maximum at annealing temperatures in the range of 200 °C–400 °C (corresponding to a grain size in the range of 30–70 nm), and decreases for higher annealing temperatures. Although this maximum is less pronounced than for Fe, the general dependence of H_c is again consistent with our description in terms of random anisotropy for small grain sizes and domain-wall pinning for larger grains.

B. Effect of oxidation: Exchange anisotropy

The temperature dependence of the coercive field (Figs. 3 and 4) shows some features that can not be readily attributed

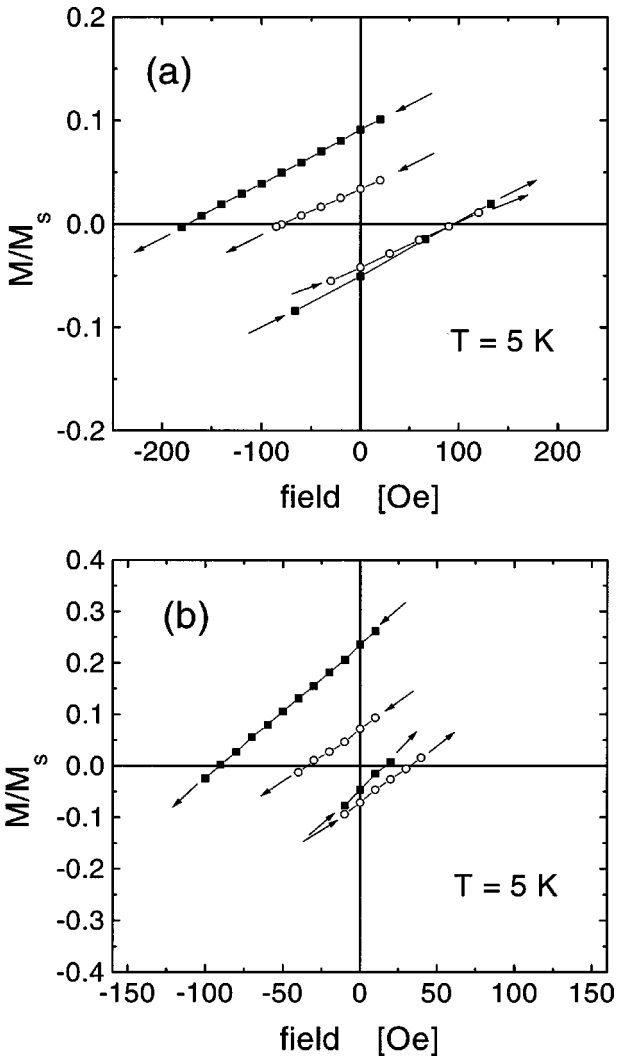

FIG. 7. Hysteresis branches around zero field, measured at a temperature of 5 K after field cooling (solid squares) and zero-field cooling (open circles); (a) as-prepared nanostructured Fe, (b) as-prepared nanostructured Ni.

to an effect of grain size or random anisotropy. These are (i) the pronounced step in H_c occurring at about 120 K in Fe after annealing at intermediate temperatures of 300 °C to 500 °C and (ii) the coercive field showing a maximum around 25 K at some stages of annealing. As our specimens have an oxygen content of between 6 and 12 at. % it is likely that these features result from the presence of oxides. This conjecture is confirmed by the fact that Fe_3O_4 undergoes a structural phase transition at 120 K, i.e., at the temperature at which a step in H_c occurs for our Fe samples. The oxides we predominantly expect are Fe_3O_4 and NiO, respectively (see also Fig. 1). Coarse-grained Fe_3O_4 is ferrimagnetic with a Curie temperature of 858 K; coarse-grained NiO is antiferromagnetic with a Néel temperature of 600 K.

As a check for the structure and influences of oxides, we measured the hysteresis loop at 5 K after the sample was cooled in an external magnetic field of 20 kOe (field cooling, FC), in contrast to the usually performed zero-field cooling (ZFC). After FC, a shift of the center of the hysteresis loop and an increase in width were observed. Figure 7 gives examples for the measured hysteresis branches around the origin for as-prepared nanocrystalline Fe (a) and Ni (b), giving evidence for a significant field displacement and spreading in width after FC, compared to ZFC where the loop is centric and narrower.

We attribute this effect to a two-phase structure where the ferromagnetic Fe or Ni grains are embedded in antiferromagnetic (or ferrimagnetic) interfacial phases of oxides. The shift of the hysteresis loop is then caused by an exchange anisotropy arising from a spin coupling between the ferromagnetic and the antiferromagnetic (or ferrimagnetic) phase. In this case an additional unidirectional anisotropy affecting the ferromagnet occurs when the sample is field cooled across the Néel temperature T_N of the antiferromagnet. Such an exchange anisotropy was discovered on fine Co particles with a CoO surface[35,36] and was also observed in several Fe based systems.[6,12,37] It is well known that the shift reduces, but does not necessarily vanish when the field cooling is performed from a starting temperature below T_N.[36,38] In the present study, the field cooling was started from room temperature in order to prevent uncontrolled grain growth in the samples.

Explanations based on considerations of exchange coupling at planar interfaces have been proposed by Néel,[39] and more sophisticated extensions are presented in Refs. 40 and 41. On the other hand, calculated spin distributions within small $NiFe_2O_4$ particles showed the existence of disordered surface spin configurations that differ from the collinear spins in the core.[42] These surface spin configurations become frozen below 50 K and are expected to be responsible for the observed shift of the FC hysteresis loop.

Figure 8 shows the shift and the change in half width between FC and ZFC of the hysteresis loop as a function of annealing temperature for the samples of Fig. 7. The shift is most pronounced in the as-prepared state and does not occur at annealing temperatures higher than 200 °C (Fe) and 500 °C (Ni); the change in half width shows the same behavior.

At *intermediate annealing temperatures* where the hysteresis shift has vanished (Fig. 8), a step of the coercive field occurs at a temperature of about 120 K (Fig. 3). At this temperature, Fe_3O_4 undergoes a phase transition.[43] The same step of the coercive field was already found in powders of small Fe_3O_4 particles.[44,45] Magnetite ($FeO \cdot Fe_2O_3$) at room temperature has an inverse spinel structure with a tendency towards dynamic disorder because of a rapid electron transfer between the Fe^{2+} and Fe^{3+} ions on the octahedral lattice sites. The magnetic phase transition to the low-temperature phase is associated with an ordering of the randomly distributed Fe^{2+} and Fe^{3+} ions[43] and with a change from cubic to orthorhombic symmetry. In this case, a lower crystal symmetry leads to a higher anisotropy constant and a higher coercive field.

Since the step occurs at annealing temperatures of 300–500 °C at which the hysteresis shift has vanished, we suggest that the oxides undergo a *restructuring* during annealing. The Fe grains, initially surrounded by oxidized interfaces, lose their oxide shell during grain growth while the oxides conglomerate to small grains of Fe_3O_4. This hypothesis is supported by the development of an Fe_3O_4 peak in the x-ray-diffraction pattern upon annealing [see inset of Fig. 1(a)]. Also for Ni, one sees a NiO peak after annealing at 550 °C

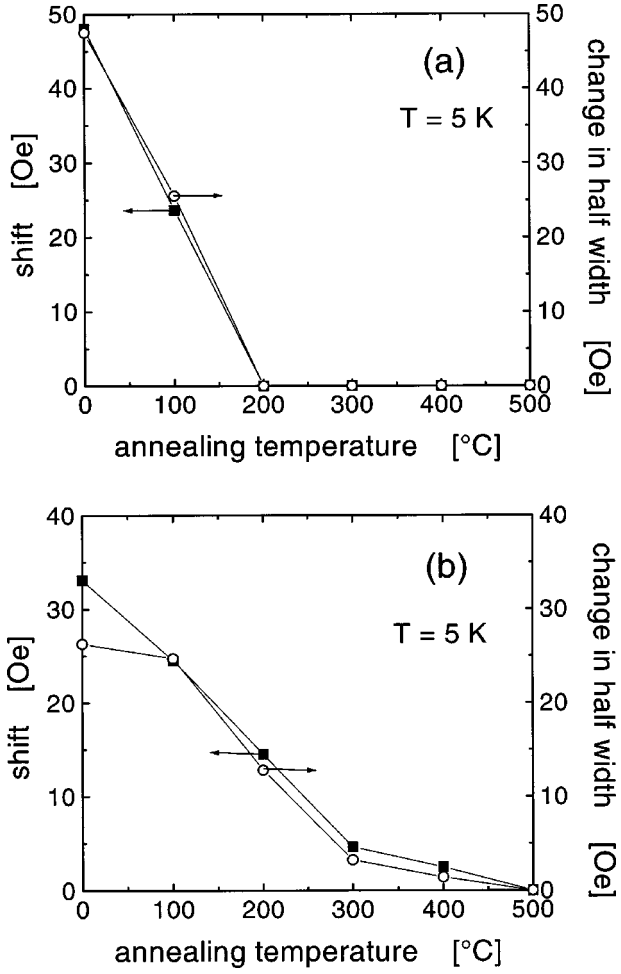

FIG. 8. Shift (solid squares) and change in half width (open circles) of the hysteresis loops as a function of annealing, measured at 5 K; (a) nanostructured Fe, (b) nanostructured Ni.

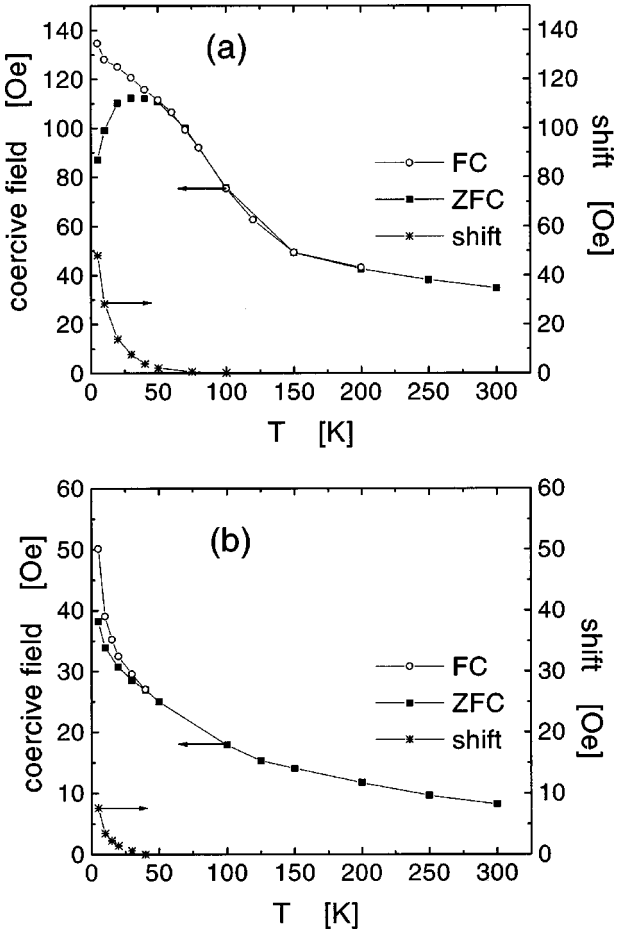

FIG. 9. Coercive field for two samples of nanostructured Fe [(a) and (b)] after zero-field cooling (ZFC) and field cooling (FC) as a function of temperature together with the field displacement of the hysteresis loop after field cooling.

[see inset of Fig. 1(b)], the temperature where the hysteresis shift has vanished (Fig. 8). Obviously, the oxides of Ni also undergo a restructuring upon annealing comparable to the oxides of Fe.

For *higher annealing temperatures* the 120 K step of the coercive field in the case of Fe vanishes, either due to the formation of FeO that is stable for temperatures above 560 °C,[18] or to the onset of multidomain behavior. In the latter case the coercive field is determined by domain-wall motions and does not primarily depend on the crystal anisotropy.

C. Temperature dependence of the coercive field

A decreasing coercive field with increasing temperature, which we observe for Fe and Ni for the as-prepared and the low-temperature annealed samples (Figs. 3 and 4), is also in general agreement with the predictions of the RAM. According to Chudnovsky,[10] the ferromagnetic correlation length increases with increasing temperature, with the consequence that the anisotropy constant is reduced by averaging over more correlated grains.

However, we see for some of our Fe and Ni samples a pronounced maximum in H_c at a specimen temperature of around 25 K. To find its origin, we investigated two as-prepared nanostructured Fe samples, one which showed this maximum and one which did not. For the sample of Fig. 9(a), H_c passes the maximum at around 25 K in the ZFC case, whereas the mean coercive field decreases monotonically with increasing temperature in the FC case. The sample of Fig. 9(b) does not exhibit a maximum in H_c but shows a monotonic decrease with increasing temperature in both cases. For this sample, the hysteresis shift is less pronounced than for the sample of Fig. 9(a). We always found the maximum in H_c correlated with a significant shift of the hysteresis whereas in the case of monotonic decrease of H_c the shift was less pronounced. We therefore attribute the peculiar behavior of H_c below 50 K to the influence of oxidized grain-boundary layers.

A similar temperature dependence of the hysteresis shift (which vanished at about 150 K) and also a maximum of the coercive field at about 100 K after oxidation were observed on nanostructured Co powder.[46] The vanishing of the shift was explained by the occurrence of superparamagnetism of the CoO grain-boundary layer with a blocking temperature identical with the temperature above which the shift disappeared. Furthermore, FC and ZFC measurements performed on nickel ferrite nanoparticles in an external field of 70 kOe showed a similar temperature dependence of the magnetiza-

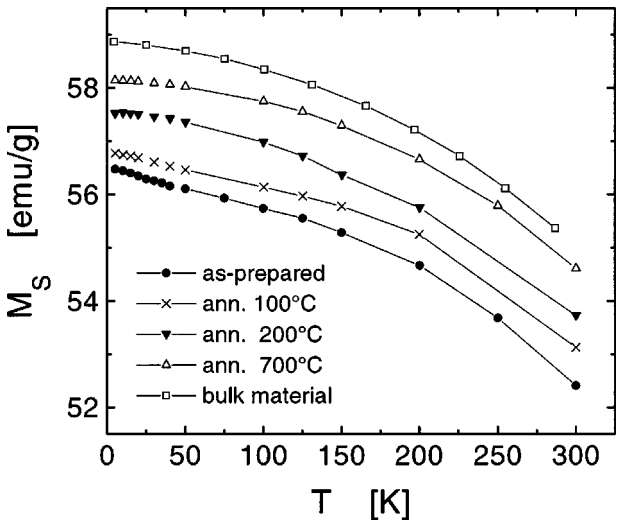

FIG. 10. Saturation magnetization of nanostructured Ni (sample #2), as a function of temperature in the as-prepared state and for different annealing steps in comparison with the literature value for coarse-grained polycrystalline Ni.

tion at this field. The magnetization at 70 kOe showed a maximum at around 25 K in the ZFC case in conjunction with a hysteresis shift in the FC case.[42,47] The behavior was explained by the freezing of disordered surface spins. Analogous to the present work, these two studies show a clear correlation between the hysteresis shift after FC and the maximum of H_c or the magnetization at 70 kOe after ZFC.

D. Saturation magnetization

Figure 10 shows the saturation magnetization M_S of nanocrystalline Ni as a function of temperature for different annealing steps in comparison with the literature values for coarse-grained polycrystalline Ni (obtained from Ref. 48). Approaching the Curie temperature, the saturation magnetization of the nanocrystalline Ni sample decreases with increasing temperature. However, in comparison with the bulk values,[48] the magnitude of the saturation magnetization here is always smaller, but increases with increasing annealing temperature.

In the context of the arguments given above, this increase with annealing (Fig. 10) may be explained equally well by (i) grain size and (ii) oxidation effects: (i) Due to the reduced atomic density in the grain-boundary region, the average magnetic moment of the grain-boundary atoms may be smaller than of those in the crystal lattice. The lowest saturation magnetization then occurs in the samples with the highest volume fraction of grain boundaries, i.e., in as-prepared samples; (ii) The restructuring of the oxides that we see in Fe and Ni upon annealing would also explain the increase of the saturation magnetization with annealing. When oxygen atoms are located in grain boundaries, the interface between the ferromagnetic Ni and the antiferromagnetic oxide phases is large compared to the case where the oxides are conglomerated in small grains. In the first case the oxygen atoms reduce the contribution of nickel atoms to the ferromagnetism more efficient than in the second case (see also Ref. 14 and references therein).

Several controversial results concerning the saturation magnetization of small particle systems are reported in the literature. A reduction of the saturation magnetization compared with the bulk value has been observed for example for nanocrystalline Ni (Ref. 13) and Gd,[49] and was explained by the structural distortions in the interfaces. In contrast, investigations of nanocrystalline Ni samples with oxygen contents reported to be about 0.5 at. % did not show this change in the saturation magnetization after annealing.[14] The saturation magnetization of nanocrystalline Ni and Fe prepared by ball milling [that generally implies less oxide formation in the interfaces than the inert-gas condensation technique (see, e.g., Ref. 32)] also showed no significant change of M_s as a function of grain size.[50,51] Furthermore, recent calculations predict that the average magnetic moment of Ni atoms in structurally different grain boundaries is only slightly reduced.[52] The low saturation magnetization in our case could therefore also be an effect of the presence of oxides in the grain boundaries apart from a grain-size effect.

IV. CONCLUSIONS

The analysis of the magnetic properties of nanostructured Fe and Ni showed the influence of grain size on the magnetic properties, and also the effect of oxides which are inherently present in our material. In our consolidated samples exchange interaction across the interfaces is possible. The random-anisotropy model was successfully applied to samples with small grain sizes. It explained the grain-size dependence of H_c and allowed to fit the approach to saturation of an as-prepared Fe sample with a grain size of 10 nm. From this fit we deduced the magnetocrystalline anisotropy constant and the ferromagnetic correlation length of the sample. The anisotropy constant we obtain from this sample is four times higher than the one known for coarse-grained Fe. The ferromagnetic correlation length, determined as 70 nm, is seven times higher than the grain size itself. For samples with grain sizes larger than 30 nm on average, the grain-size dependence of the magnetic properties is comparable with that of coarse-grained ferromagnetic materials. The coercive field follows a $1/D$ behavior, a relation that is generally ascribed to the pinning of domain walls at interfaces.

The hysteresis shift measured after cooling the material in an external field is accounted for by a two-phase model where the ferromagnetic Fe or Ni grains are embedded in antiferromagnetic (or ferrimagnetic) interfacial phases of oxides. Upon annealing we find a restructuring of the oxides such that the Fe and Ni grains, originally surrounded by oxidized interfaces, lose their oxide shell during grain growth while the oxides conglomerate to small grains. This hypothesis is confirmed by x-ray diffraction and magnetization measurements.

The temperature dependence of the coercive field as well as the reduced saturation magnetization of the as-prepared Fe and Ni samples is also explained by grain size and oxidation effects. For some of our nanostructured Fe and Ni samples we observe a maximum in the coercive field at about 25 K correlated with a pronounced hysteresis shift after field cool-

ing. We explain this observation by the influence of oxidized grain-boundary layers. The reduced saturation magnetization of the samples with small grain sizes may also be attributed to the two-phase structure of the system, in addition to the possible influence of the small grain size itself on the saturation magnetization.

ACKNOWLEDGMENTS

This work was supported by the Schweizerischen Nationalfonds zur Förderung der wissenschaftlichen Forschung; J.L. also acknowledges general support by the Studienstiftung des deutschen Volkes.

[1] C. P. Bean, J. Appl. Phys. **26**, 1381 (1955).
[2] B. D. Cullity, *Introduction to Magnetic Materials* (Addison-Wesley, Reading, MA, 1972).
[3] S. Chikazumi, *Physics of Magnetism* (Wiley, New York, 1964).
[4] The first and the third category may overlap at some temperatures such that the second one does not always exist.
[5] E. F. Kneller and F. E. Luborsky, J. Appl. Phys. **34**, 656 (1963).
[6] S. Gangopadhyay, G. C. Hadjipanayis, B. Dale, C. M. Sorensen, K. J. Klabunde, V. Papaefthymiou, and A. Kostikas, Phys. Rev. B **45**, 9778 (1992).
[7] Gang Xiao, S. H. Liou, A. Levy, J. N. Taylor, and C. L. Chien, Phys. Rev. B **34**, 7573 (1986).
[8] *Proceedings of the 2nd International Conference on Nanostructured Materials*, edited by H.-E. Schaefer, R. Würschum, H. Gleiter, and T. Tsakalakos [Nanostruct. Mater. **6** (1995)]; *Proceedings of the 3rd International Conference on Nanostructured Materials*, edited by M. Trudeau, V. Provenzano, R. Shull, and J. Ying [Nanostruct. Mater. **9** (1997)].
[9] R. Alben, J. J. Becker, and M. C. Chi, J. Appl. Phys. **49**, 1653 (1978).
[10] Eugene M. Chudnovsky, in *The Magnetism of Amorphous Metals and Alloys*, edited by J. A. Fernandez-Baca and Wai-Yim Ching (World Scientific, Singapore, 1995), Chap. 3.
[11] E. M. Chudnovsky, W. M. Saslow, and R. A. Serota, Phys. Rev. B **33**, 251 (1986).
[12] J. P. Perez, V. Dupuis, J. Tuaillon, A. Perez, V. Paillard, P. Melinon, M. Treilleux, L. Thomas, B. Barbara, and B. Bouchet-Fabre, J. Magn. Magn. Mater. **145**, 74 (1995).
[13] H. E. Schäfer, H. Kisker, H. Kronmüller, and R. Würschum, Nanostruct. Mater. **1**, 523 (1992).
[14] H. Kisker, T. Gessmann, R. Würschum, H. Kronmüller, and H. E. Schäfer, Nanostruct. Mater. **6**, 925 (1995).
[15] R. Birringer, H. Gleiter, H.-P. Klein, and P. Marquardt, Phys. Lett. **102A**, 365 (1984).
[16] H. Gleiter, Prog. Mater. Sci. **33**, 223 (1989).
[17] H. P. Klug and L. E. Alexander, *X-Ray Diffraction Procedures for Polycrystalline and Amorphous Materials*, 2nd ed. (Wiley, New York, 1974), pp. 661–665.
[18] J. B. Goodenough, W. Gräper, F. Holtzberg, D. L. Huber, R. A. Lefever, J. M. Longo, T. R. McGuire, and S. Methfessel, in *Magnetic and Other Properties of Oxides and Related Compounds*, edited by K.-H. Hellwege and A. M. Hellwege, Landolt-Börnstein, Group III, Vol. 4a (Springer, Berlin, 1970), p. 7.
[19] A. Mager, Ann. Phys. (Leipzig) **11**, 15 (1952).
[20] J. Degauque, B. Astié, J. L. Porteseil, and R. Vergne, J. Magn. Magn. Mater. **26**, 261 (1982).
[21] F. Pfeifer and C. Radeloff, J. Magn. Magn. Mater. **19**, 190 (1980).
[22] K. Adachi, D. Bonnenberg, J. J. M. Franse, R. Gersdorf, K. A. Hempel, K. Kanematsu, S. Misawa, M. Shiga, M. B. Stearns, and H. P. J. Wijn, in *Magnetic Properties of Metals*, edited by H. P. J. Wijn, Landolt-Börnstein, Group III, Vol. 19a (Springer, Berlin, 1986), p. 42.
[23] M. E. Schabes, J. Magn. Magn. Mater. **95**, 249 (1991).
[24] Eugene M. Chudnovsky, J. Appl. Phys. **64**, 5770 (1988).
[25] G. Herzer, J. Magn. Magn. Mater. **112**, 258 (1992).
[26] G. Herzer, Scr. Metall. Mater. **33**, 1741 (1995).
[27] J. Filippi, V. S. Amaral, and B. Barbara, Phys. Rev. B **44**, 2842 (1991).
[28] E. M. Chudnovsky and R. A. Serota, J. Phys. C **16**, 4181 (1983).
[29] S. U. Jen, C. Y. Lee, Y. D. Yao, and K. C. Lee, J. Magn. Magn. Mater. **96**, 82 (1991).
[30] N. Hassanain, H. Lassri, R. Krishnan, and A. Berrada, J. Magn. Magn. Mater. **146**, 315 (1995).
[31] M. W. Grinstaff, M. B. Salamon, and K. S. Suslick, Phys. Rev. B **48**, 269 (1993).
[32] J. Löffler, W. Wagner, H. Van Swygenhoven, and A. Wiedenmann, Nanostruct. Mater. **9**, 331 (1997).
[33] H.-B. Braun and H. N. Bertram, J. Appl. Phys. **75**, 4609 (1994).
[34] This equation differs by a factor of 2 from the one given in Ref. 33 where the stiffness against the formation of domain-wall *pairs* is considered.
[35] W. H. Meiklejohn and C. P. Bean, Phys. Rev. **102**, 1413 (1956).
[36] W. H. Meiklejohn and C. P. Bean, Phys. Rev. **105**, 904 (1957).
[37] C. Schlenker and D. Paccard, J. Phys. (France) **28**, 611 (1967).
[38] W. H. Meiklejohn, J. Appl. Phys. **33**, 1328 (1962).
[39] L. Néel, Ann. Phys. (Paris) **2**, 61 (1967).
[40] A. P. Malozemoff, Phys. Rev. B **35**, 3679 (1987).
[41] A. P. Malozemoff, J. Appl. Phys. **63**, 3874 (1988).
[42] R. H. Kodama, A. E. Berkowitz, E. J. McNiff, Jr., and S. Foner, Phys. Rev. Lett. **77**, 394 (1996).
[43] E. J. Verwey, P. W. Haayman, and F. C. Romeijn, J. Chem. Phys. **15**, 181 (1947).
[44] D. B. Bonstrom, A. H. Morrish, and L. A. K. Watt, J. Appl. Phys. **32**, 272S (1961).
[45] E. Schmidbauer and R. Keller, J. Magn. Magn. Mater. **152**, 99 (1996).
[46] S. Gangopadhyay, G. C. Hadjipanayis, C. M. Sorensen, and K. J. Klabunde, Nanostruct. Mater. **1**, 449 (1992).
[47] R. H. Kodama, A. E. Berkowitz, E. J. McNiff, Jr., and S. Foner, Mater. Sci. Forum **235-238**, 643 (1997).
[48] K. Adachi *et al.*, in *Magnetic Properties of Metals* (Ref. 22), p. 35.
[49] C. E. Krill, F. Merzoug, W. Krauss, and R. Birringer, Nanostruct. Mater. **9**, 455 (1997).
[50] L. Daróczi, D. L. Beke, G. Posgay, G. F. Zhou, and H. Bakker, Nanostruct. Mater. **2**, 515 (1993).
[51] L. Daróczi, D. L. Beke, G. Posgay, and M. Kis-Varga, Nanostruct. Mater. **6**, 981 (1995).
[52] B. Szpunar, U. Erb, G. Palumbo, K. T. Aust, and L. J. Lewis, Phys. Rev. B **53**, 5547 (1996).